THE JOURNAL OF PHYSICAL CHEMISTRY Letters

pubs.acs.org/JPCL Letter

Graphene Plasmonics: Fully Atomistic Approach for Realistic Structures

Tommaso Giovannini,[⊥] Luca Bonatti,[⊥] Marco Polini, and Chiara Cappelli*

Cite This: *J. Phys. Chem. Lett.* 2020, 11, 7595−7602 Read Online

ACCESS | Metrics & More | Article Recommendations | Supporting Information

ABSTRACT: We demonstrate that the plasmonic properties of realistic graphene and graphene-based materials can effectively and accurately be modeled by a novel, fully atomistic, yet classical, approach, named ωFQ. Such a model is able to reproduce all plasmonic features of these materials and their dependence on shape, dimension, and fundamental physical parameters (Fermi energy, relaxation time, and two-dimensional electron density). Remarkably, ωFQ is able to accurately reproduce experimental data for realistic structures of hundreds of nanometers (∼370k atoms), which cannot be afforded by any *ab initio* method. Also, the atomistic nature of ωFQ permits the investigation of complex shapes, which can hardly be dealt with by exploiting widespread continuum approaches.

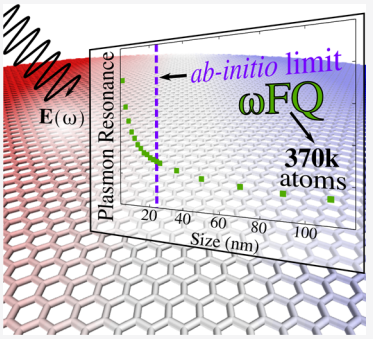

Graphene[1] has emerged as an outstanding plasmonic material[2,3] because it provides a strong field confinement with relatively low losses[4] that cannot be reached by noble metal plasmons.[5] Additionally, graphene plasmons can be easily tuned by exploiting electrical gating.[6−14] Such a unique property, together with the possibility of chemical doping, provides an easy mechanism to tune the Fermi energy in graphene[15] and consequently the plasmon resonance frequency (PRF). In this context, an accurate modeling of the optical response of both homogeneous and nanopatterned graphene is of crucial relevance in the development of devices or in the understanding of complex physical phenomena, as for instance in graphene enhanced Raman scattering (GERS).[16−19]

The optical properties of graphene have been so far computationally investigated[10,20−26] by exploiting continuum classical approaches (e.g., the boundary element method, BEM)[20,22,27] or *ab initio* methods.[21,28,29]

Continuum models have low computational cost,[10] but they lack any atomistic description of the 2D material and therefore cannot describe finite-size, edge effects[23] and defects. The latter can indeed be treated by *ab initio* methods,[23,24,30−32] but at a high computational cost, which hampers the study of large, realistic structures.

In this work, we present a novel, fully atomistic, yet classical, approach (named ωFQ) able to reproduce all plasmonic features of graphene and graphene-based materials. Remarkably, our method overcomes most of the limitations of current continuum and *ab initio* methods; in fact, it gives results quantitatively comparable to *ab initio* but for large, realistic structures of more than ∼370k atoms, which can normally be tackled only with continuum models, because they are completely not affordable by *ab initio* approaches. Large systems can in principle be described by means of continuum approaches; however, in the case of complex shapes, basic electrodynamical continuum methods cannot be applied and numerical methodologies (such BEM) able to treat complex boundaries need to be exploited.[33] Their use is far from trivial, thus limiting their application in realistic systems.

ωFQ finds its theoretical foundations in the fact that the plasmonic response of 2D carbon-based materials is dominated by the synchronous excitation of π electrons, which is mediated by the electrodynamical conductance. In this framework, in ωFQ each graphene carbon atom is endowed with electric charge q_i, whose value is not fixed but varies as a response to the external oscillating electric field. In order to effectively calculate absorption properties, ωFQ charges q_i need to be defined as complex (i.e., real + imaginary) quantities, and their imaginary part is related to absorption phenomena. The classical equation of motion which specifies the charges is obtained by modeling the charge exchange as regulated by the Drude model, which mimics the electrodynamical conductance. The charge flow between atoms then occurs because of the difference in their chemical potential.[34]

In the frequency domain, the classical ωFQ equation of motion for charges reads as follows (see the Supporting Information for the complete derivation):

Received: July 3, 2020
Accepted: August 17, 2020
Published: August 17, 2020

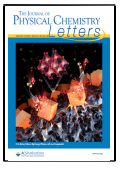

https://dx.doi.org/10.1021/acs.jpclett.0c02051
J. Phys. Chem. Lett. 2020, 11, 7595−7602

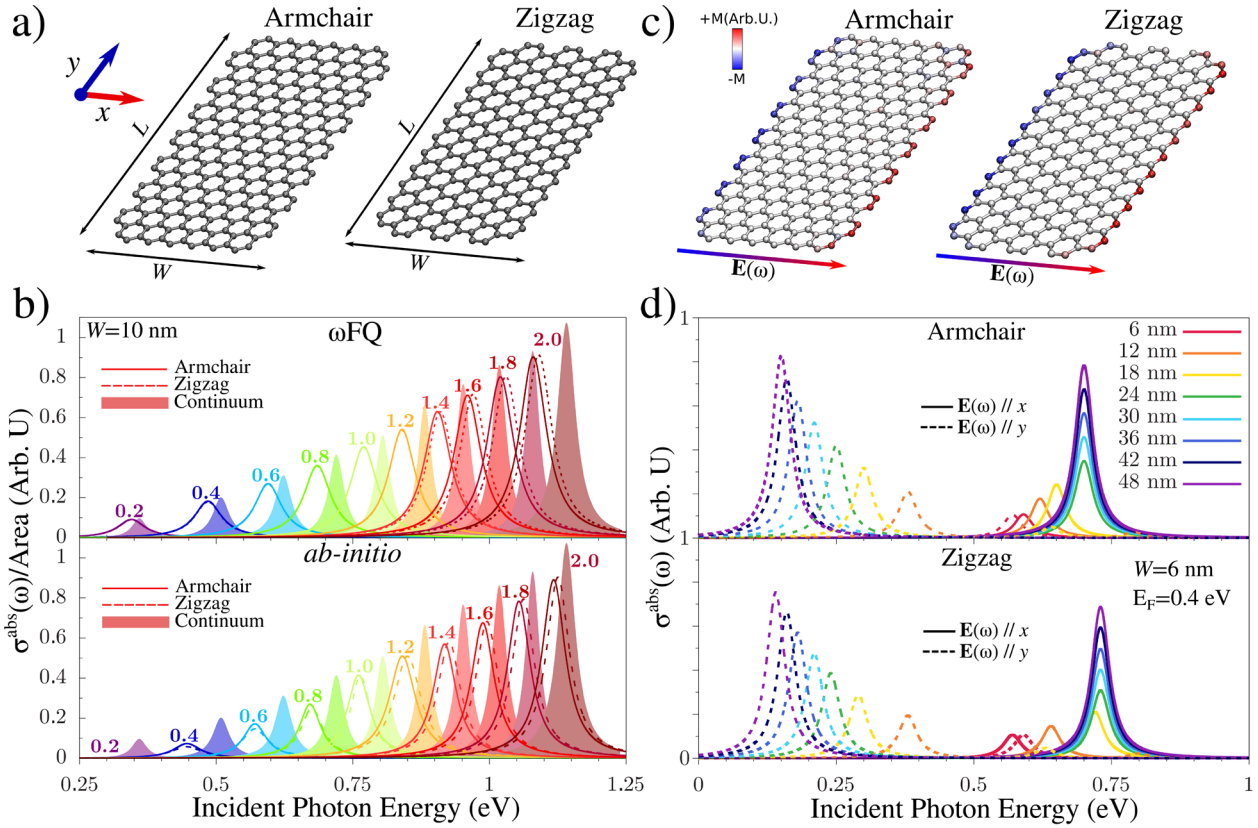

Figure 1. (a) Graphical depiction of the armchair and zigzag graphene nanoribbons studied in the present work. The two characteristic length scales W (short edge) and L (long edge) are highlighted. (b) ωFQ (top) and *ab initio* (bottom) σ^{abs} of a graphene nanoribbon (W = 10 nm and L = 12 nm) as a function of the Fermi energy (E_F) (from 0.2 to 2.0 eV, with a constant step of 0.2 eV). Classical continuum results are also reported. Both classical continuum and *ab initio* data are reproduced from ref 24. In all cases, x-polarization is considered. (c) Pictorial representation of ωFQ imaginary charges representing the local plasmonic response for AC and ZZ nanoribbons. Colors are saturated for $\pm 3.0^{-1}$ a.u. The external electric field intensity is 10^{-7} a.u. (d) ωFQ σ^{abs} of armchair (top) and zigzag (bottom) graphene nanoribbons (W = 6 nm) as a function of L (from 6 nm (squared graphene sheet) to 48 nm, with a constant step of 6 nm). Both x- (solid line) and y- (dashed line) polarizations are considered. E_F is 0.4 eV in all calculations.

$$-i\omega q_i = \frac{2\tau v_F}{1 - i\omega\tau}\sqrt{\frac{n_{2D}}{\pi}}\sum_j f(l_{ij})\cdot\frac{A_{ij}}{l_{ij}}\cdot(\mu_j^{el} - \mu_i^{el}) \quad (1)$$

where ω is the frequency of the external electric field, τ the relaxation time, v_F the Fermi velocity (fixed to 10^6 m/s), and n_{2D} the 2D-density of graphene. A_{ij} is the effective area connecting the ith and jth atoms, l_{ij} their distance, and μ_i^{el} the electrochemical potential of atom i. The Fermi energy is defined as $E_F = \hbar v_F\sqrt{\pi\cdot n_{2D}}$, whereas the effective mass $m^* = \sqrt{\pi\cdot n_{2D}}/v_F$.[35] Finally, $f(l_{ij})$ is a function that guarantees that charge exchange occurs only between nearest neighbor atoms. As it can be seen by eq 1, ωFQ finds its strengths in the simplicity of the formulation and in the fact that the different parameters entering eq 1 can be directly recovered from experimental and/or computed data (see Table S4 in the Supporting Information), thus potentially allowing its extension to 2D materials other than carbon-based samples. In addition, its fully atomistic nature permits treating structural defects and/or chemical doping by simply modifying the input geometrical structures and parameters.

In this work, the potentialities and the performance of ωFQ are shown for four challenging, differently shaped graphene-based materials (nanoribbons, nanotriangles, nanodisks, and nanorings). All the studied structures are planar and have been constructed by fixing the carbon−carbon distance (1.42 Å).[35] Notice that the 2D-density (n_{2D}) depends on the area of the material; therefore, purely geometrical differences on the target systems directly reflect on the definition of n_{2D} and indirectly on atom−atom couplings.

We first show the performance of ωFQ as applied to the optical response of graphene-based nanoribbons and nanotriangles, in two possible edge configurations, namely armchair-AC and zigzag-ZZ (see Figures 1 and 2, panel a). Note that the atomistic nature of ωFQ allows discriminating between the two geometrical arrangements.

The absorption cross section (σ^{abs}) of AC and ZZ nanoribbons with W = 10 nm and L = 12 nm (see Figure 1a for definition) was computed as a function of the Fermi energy (E_F, see Figure 1b): modifications in E_F are widely exploited experimentally to tune the plasmonic response of graphene-based materials. Remarkably, because of its physical relevance, E_F enters the definition of ωFQ response equations (see the Supporting Information). ωFQ absorption cross sections are compared with both classical-continuum and atomistic *ab initio* descriptions of the graphene-sheet, taken from ref 24.

The absorption cross section calculated by exploiting ωFQ shows a prominent plasmon band which rapidly decreases in intensity and redshifts as E_F decreases from 2.0 to 0.2 eV (see Figure 1b, top). The nature of the plasmon responsible for the observed peak was investigated by plotting the imaginary ωFQ charges calculated at the PRF for both AC and ZZ

https://dx.doi.org/10.1021/acs.jpclett.0c02051
J. Phys. Chem. Lett. 2020, 11, 7595−7602

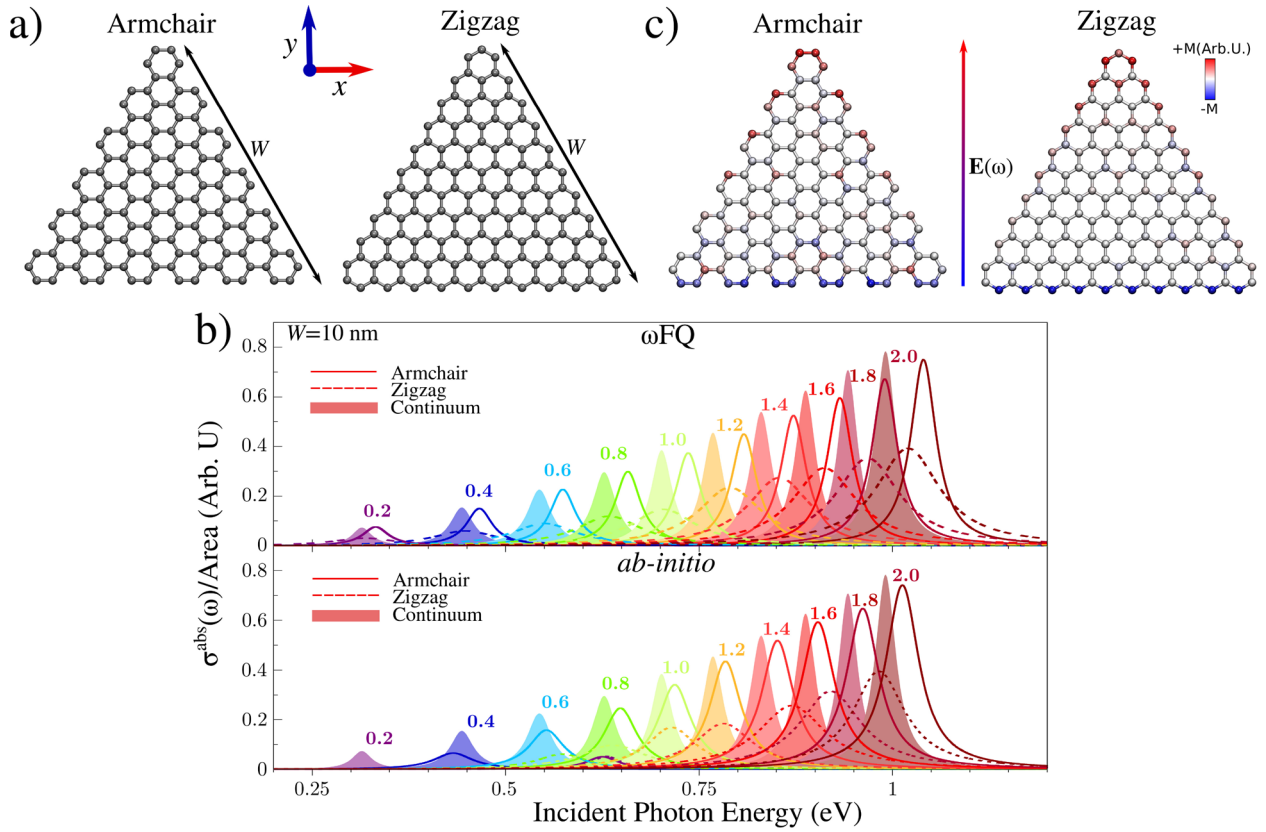

Figure 2. (a) Graphical depiction of the armchair and zigzag graphene nanotriangles studied in the present work. The main length scale (edge length) W is highlighted. (b) ωFQ (top) and *ab initio* (bottom) σ^{abs} of a graphene nanotriangle (W = 10 nm) as a function of the Fermi energy (E_F) (from 0.2 to 2.0 eV, with a constant step of 0.2 eV). Classical continuum results are also reported. Both classical continuum and *ab initio* data are reproduced from ref 24. In all cases, y-polarization is considered. (c) Pictorial representation of ωFQ imaginary charges representing the local plasmonic response for AC and ZZ nanotriangles. Colors are saturated for $\pm 3.0^{-1}$ a.u. The external electric field intensity is 10^{-7} a.u.

configurations (see Figure 1c): as is shown by its associated charge distribution, this peak arises from a collective excitation of the electrons of the systems, and in particular, it is a dipolar plasmon. By examining in depth Figure 1b, ωFQ calculations are in almost perfect agreement with *ab initio* data for both structural arrangements,[24] provided that E_F is greater than PRF. Under such conditions, ωFQ correctly reproduces the small differences between AC and ZZ edges, which are predicted by *ab initio* data, and this is particularly evident for E_F > 1.0 eV. This is indeed impressive and highlights the capabilities of our fully atomistic method to accurately describe edge effects on the plasmonic response. Remarkably, the continuum approach cannot distinguish between AC and ZZ configurations because of its intrinsic limitations, which hamper a proper description of edge effects. The major discrepancies between ωFQ and *ab initio* are reported if PRF > E_F; however, this does not influence the overall qualitative behavior of computed ωFQ results. Note also that the observed trends are not surprising and are due to quantum effects which are not included in classical approaches such as ωFQ or continuum approaches.[24]

As stated before, one of the main features of graphene-based materials is the possibility to tune their optical response by modifying structural and electronic properties. Figure 1d reports calculated ωFQ absorption cross sections of AC and ZZ graphene nanoribbons with W = 6 nm, as a function of both the length of the sheet ($6 \le L \le 48$ nm) and the direction of the external electric field (either x- or y-polarizations). In the case of x- polarization (see Figure 1d, solid lines), the PRF remains almost constant if the aspect ratio (i.e., L/W) is above 4 (L = 24 nm, green line), independent of the considered configuration. In contrast, PRF redshifts for smaller structures. The same does not apply to y-polarization (see Figure 1d, dashed lines), for which PRF shifts to lower energies with respect to x-polarization. Also, PRF redshifts as the length of the nanoribbon increases. Such a behavior is perfectly in line with what is expected for an infinite nanoribbon with fixed width (W), which is characterized by a propagating plasmon. Therefore, the effects we are pointing out for y-polarization are entirely due to finite size effects. We notice also that, although computed imaginary polarizabilities are almost three times larger for y-polarization (as it is expected because the longer path of the dipolar plasmon lies on y direction, see Figure S4 in the Supporting Information), σ^{abs} is almost identical for the two perpendicular polarizations, because of its definition in terms of the external frequency (see Supporting Information). Therefore, a change in the field polarization allows for an alternative mechanism to tune the PRF of graphene nanoribbons. To the best of our knowledge, this aspect has not been attentively investigated in previous literature.[36]

We now move to discuss graphene-based nanotriangles (see Figure 2) in both AC and ZZ configurations (see Figure 2a, in which the main dimension W is also highlighted). In Figure 2b, calculated ωFQ absorption cross sections are reported for a nanotriangle with W = 10 nm as a function of E_F. *Ab initio* and continuum reference calculations, reproduced from ref 24, are

https://dx.doi.org/10.1021/acs.jpclett.0c02051
J. Phys. Chem. Lett. 2020, 11, 7595−7602

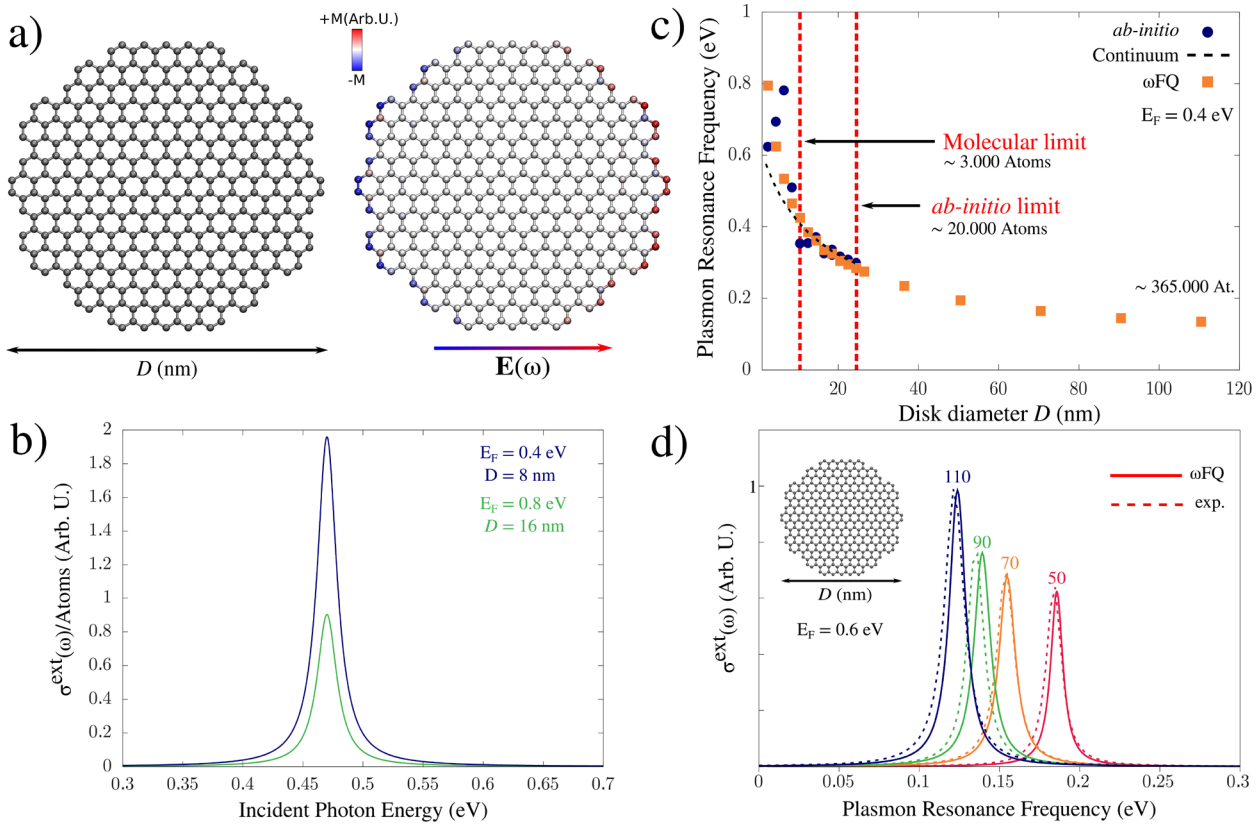

Figure 3. (a) Graphical depiction of the graphene disks studied in the present work. The main length scale D (diameter length) is highlighted (left). Pictorial representation of ωFQ imaginary charges representing the local plasmonic response of graphene disks (right). Colors are saturated for $\pm 3.0^{-1}$ a.u. The external electric field intensity is 10^{-7} a.u. (b) ωFQ σ^{ext} of two graphene disks (D = 8 nm and D = 16 nm, respectively) calculated by imposing E_F equal to 0.4 and 0.8 eV respectively. (c) ωFQ (square orange points) and *ab initio* (random phase approximation, RPA; circle points) plasmon resonance frequency (eV) as a function of D (from 2 to 110 nm). Classical continuum results are also depicted (dashed line). Both continuum and *ab initio* data are reproduced from ref 23. E_F is 0.4 eV in all calculations. (d) ωFQ σ^{ext} of graphene disks with different diameter lengths (from 50 to 110 nm). The experimental data are reproduced from ref 10. E_F is 0.6 eV. ωFQ spectra are corrected by the factor $1/\sqrt{\epsilon}$, with $\epsilon = \frac{1+\varepsilon_{SiO_2}}{2}$, ε_{SiO_2} = 2.30.[10]

also shown for a direct comparison. Similarly to the previous case, the ωFQ absorption cross section is dominated by a band which rapidly redshifts and decreases in intensity by decreasing E_F. In contrast to nanoribbons, large differences are obtained between AC and ZZ band widths, which reflect the different scattering times (τ) associated with this particular structures (see Table S4).[24] Also, this time ZZ PRFs are red-shifted with respect to AC ones. The plasmon modes associated with the main band are plotted in terms of the imaginary ωFQ charges for both AC and ZZ configurations in Figure 2c. Also in this case plasmon modes have a dipolar character.

Remarkably, all features of ωFQ spectra are entirely confirmed by reference *ab initio* data[24] (see Figure 2b, bottom). The agreement with our atomistic, yet classical, approach is impressive, and only a small blueshift of the ωFQ PRFs with respect to their reference counterparts is noticed. However, such a discrepancy can be arbitrarily reduced by modifying ωFQ parameters, which have been set to give the best agreement for all studied geometries on average (see Figure S1 in the Supporting Information). Similarly to nanoribbons, the electromagnetic simulations cannot reproduce the differences between AC and ZZ configurations, which are instead well described by ωFQ. Finally, it is also worth noticing that ωFQ correctly reproduces the degeneracy between x- and y-polarizations (see Figure S5 in the Supporting Information), a feature which has recently been reported for similar geometries.[37]

As a third case study, ωFQ is challenged against graphene-based disks of diameter D. Such nanodisks have been constructed by following the same procedure as described in ref 23 (see Figure 3a, left). First, we selected two nanodisks with D equal to 8 or 16 nm; their optical response was calculated by choosing E_F = 0.4 and E_F = 0.8 eV, respectively (see Figure 3b). Both calculated ωFQ spectra are characterized by an intense peak at about 0.47 eV. The plasmonic character of the associated plasmon is depicted in Figure 3a, right, showing again the typical dipolar plasmon. The capability of ωFQ to yield identical PRFs for the two studied systems confirms its robustness and reliability. In fact, the peculiar property of graphene-based materials to yield plasmon degeneracy as a result of a modulation by the same numerical factor (in this case 2) of both the intrinsic dimensions of the considered substrate and the Fermi energy is correctly reproduced.[38] Also, the computed decreasing of the normalized extinction cross section σ^{ext} (given by the sum of σ^{abs} and the scattering cross section) is in perfect agreement with previous *ab initio* studies on similar graphene-based structures.[23,38]

The dependence of the calculated ωFQ PRF on the disk diameter is reported in Figure 3c (orange squares) together

https://dx.doi.org/10.1021/acs.jpclett.0c02051
J. Phys. Chem. Lett. 2020, 11, 7595−7602

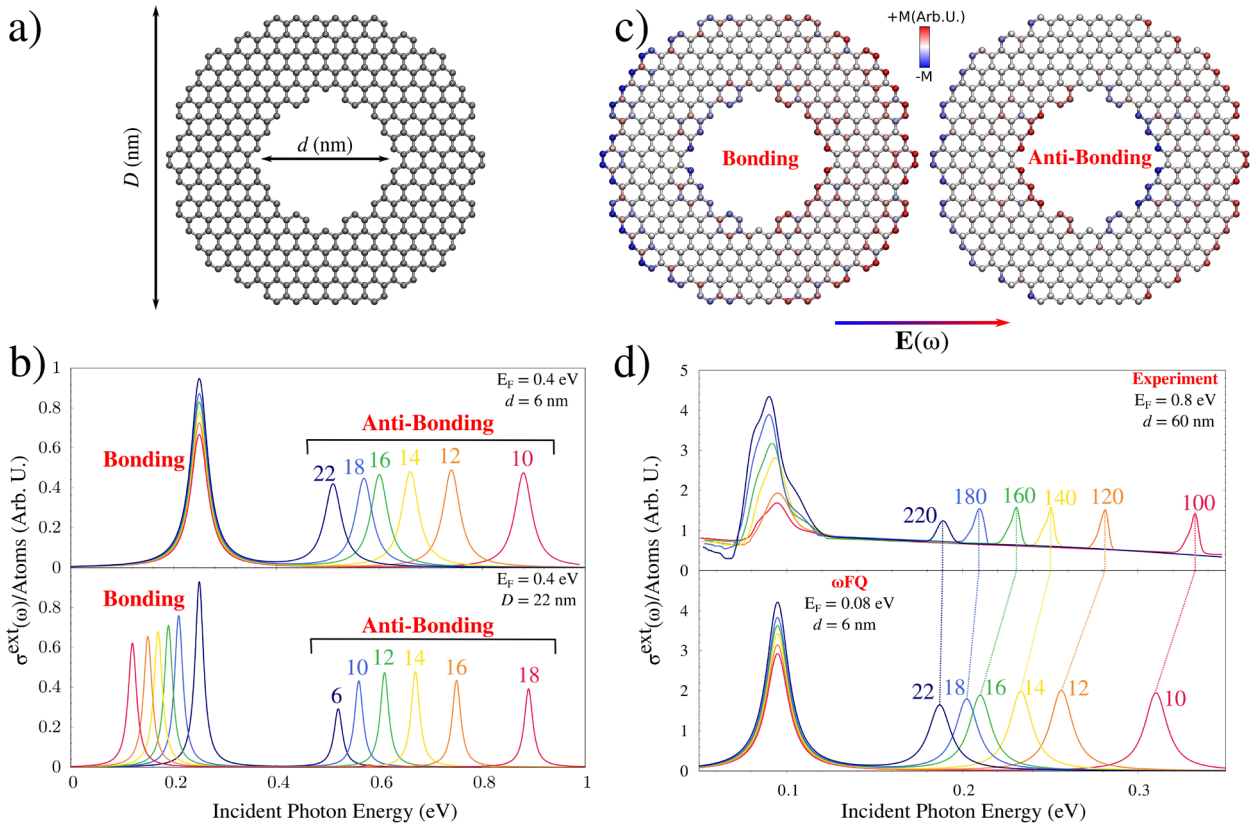

Figure 4. (a) Graphical depiction of graphene rings studied in the present work. The two relevant length scales D (external diameter length) and d (internal diameter length) are highlighted. (b) ωFQ σ^{ext} of graphene rings with fixed d = 6 nm (top) and D = 22 nm (bottom) as a function of D (top) and d (bottom). The length of the varied diameter is reported above each peak (in nm). Bonding and anti-bonding plasmon modes are highlighted. The Fermi energy is 0.4 eV. (c) Pictorial representation of ωFQ imaginary charges representing bonding (left) and antibonding (right) local plasmonic response for graphene rings. Colors are saturated for $\pm 3.0^{-1}$ a.u. The external electric field intensity is 10^{-7} a.u. (d) Experimental[10] (top) and computed ωFQ (bottom) σ^{ext} of graphene rings with fixed d = 60 nm (top) and d = 6 nm (bottom) as a function of D (from 220 to 100 nm, top; from 22 to 10 nm, bottom). The length of the varied diameter D is reported above each peak (in nm). The experimental E_F in the experiment is 0.8 eV (top), whereas ωFQ E_F is 0.08 eV (bottom). ωFQ spectra are corrected by the factor $1/\sqrt{\epsilon}$, with $\epsilon = \frac{1+\varepsilon_{SiO_2}}{2}$ and ε_{SiO_2} = 2.30.[10]

with *ab initio* (blue circles) and continuum BEM (dashed line) data reproduced from ref 23. *Ab initio* and BEM results are limited to disk diameters from 2 nm (112 atoms) to 24 nm (17 272 atoms).[23] The Fermi energy is fixed to 0.4 eV. For D > 14 nm, the ωFQ PRF perfectly matches both *ab initio* and BEM data. In particular, ωFQ and BEM values are almost identical for D > 8 nm, whereas the matching with *ab initio* values occurs for D > 14 nm. We notice that the small redshifts/blueshifts reported for some structures with D > 14 nm at the *ab initio* level with respect to BEM are correctly reproduced by ωFQ, thus confirming once again its capability to take into account the effects arising from small structural differences. When the diameter is less than 8 nm, both *ab initio* and ωFQ deviate from the BEM continuum curve; in particular, a large blueshift arises, which is almost 0.2 eV for D = 2 nm at the ωFQ level. However, for such small structures, the reference *ab initio* results do not present a clear trend as a function of the disk diameter, thus probably showing that the molecular limit is reached.[23] As a consequence, ωFQ cannot exactly reproduce the *ab initio* trend because the Drude model may fail in the limit of molecular excitations which are ruled by quantum mechanics.[23,39] In Figure 3c, ωFQ PRF are also plotted for disks with D > 24 nm, which is the largest structure affordable by *ab initio* methods.[23] Clearly, ωFQ allows the calculation of structures that are more than 20 times greater than those affordable by state-of-the-art approaches.[23,24] The plasmonic modes occurring in this range of dimensions are obviously well-described by classical approaches (such as BEM and ωFQ). However, the atomistic nature of ωFQ permits the investigation of complex geometrical arrangements, which can be hardly faced with purely continuum approaches.

To further demonstrate ωFQ reliability and potentialities, in Figure 3d we compare our results with experimental σ^{ext} data measured for graphene-based disks with 50 nm < D < 110 nm.[10] Notice that such experimental measurements were conducted on graphene disks patterned on an ITO-coated silica substrate and covered with ion gel.[10] Notice that in ωFQ, we have that $\sigma^{abs} \propto \frac{1}{\sqrt{\epsilon}}$, where ϵ is the relative permittivity constant of the surrounding environment.[2] Therefore, in order to match experimental conditions,[10] ϵ has been replaced by $\frac{1+\varepsilon_{SiO_2}}{2}$, where ε_{SiO_2} is the permittivity constant of SiO_2 (i.e., 2.3).[10] By looking at Figure 3d, the agreement between computed and experimental data is impressive, and both peak relative positions and relative intensities perfectly match experimental values (with an error of about 0.01 eV).

As a last example, we applied ωFQ to the calculation of the optical response properties of graphene-based rings, which are

https://dx.doi.org/10.1021/acs.jpclett.0c02051
J. Phys. Chem. Lett. 2020, 11, 7595−7602

obtained by cutting an inner disk of diameter d from a bigger disk of diameter D (see Figure 4a). Such a system was chosen to show that PRF can be tuned by modifying the internal diameter (d) and keeping fixed the external one (D) and *vice versa*. In Figure 4b, σ^{ext} for a ring with d equal to 6 nm (top) and with D equal to 22 nm (bottom) was studied as a function of D (top) and d (bottom), respectively. In the former case, the spectrum is dominated by an intense peak at about 0.24 eV, whose PRF remains constant by changing D, and by a second band at higher energy which redshifts as D increases (see Figure 4b, top). In the second case (i.e., D = 22 nm as a function of d, see Figure 4b, bottom), the two bands are still present, but they show opposite trends as the dimension of the structure increases, i.e. the first blueshifts (PRF < 0.3 eV) whereas the second reshifts (PRF > 0.45 eV). In both cases, we studied the plasmonic nature of the two plasmon modes associated with the two bands by resorting to the so-called hybridization model,[40,41] which have been amply exploited to theoretically explain the plasmon excitations arising in structures presenting cavities.[10,40−45] In particular, by plotting the imaginary ωFQ charges calculated at the two PRFs we see that the typical bonding and antibonding modes, which are theoretically predicted by hybridization models, are perfectly described by ωFQ. In Figure 4b, the two bands are labeled and assigned to the two plasmonic modes.

ωFQ results are finally compared to the experimentally measured dependence of σ^{ext} on D for selected graphene-based rings with d equal to 60 nm. D varies from 100 to 220 nm, and the experimental Fermi energy is set to 0.8 eV. Similar to the previous case (graphene disks), in the experimental measurements graphene rings were patterned on ITO-coated silica substrate and covered with ion gel.[10] Therefore, the same approach sketched above to correct σ^{abs} has been exploited. To demonstrate the reliability of ωFQ, we exploited the degeneracy property exposed above for nanodisks (see Figure 3b). Therefore, we have multiplied by the same numerical factor both the intrinsic dimensions of the nanostructure (d, D) and the Fermi energy. In this particular case, such a degeneracy is obtained by dividing both the aforementioned quantities by 10, so that the studied rings are exactly the same as those discussed in Figure 4b, but the Fermi energy this time is set to 0.08 eV. The agreement between the experimental[10] and computed ωFQ extinction cross sections is particularly impressive, considering that all the most relevant experimental quantities (PRF of bonding and antibonding modes) are almost perfectly reproduced by ωFQ (see Figure 4d). Notice however that some discrepancies, in particular in the case of the antibonding modes (above 0.2 eV), are present. These can be due to finite size effects of the computationally considered structures. As a last comment, we want to stress that ωFQ can in principle afford experimental structures (which are constituted of ∼600 000 atoms at most, for the largest structure). However, instead of showing the calculated data for the actual structures in this case we show that it is possible to hugely reduce the computational cost of the calculation, but keep the same accuracy with the actual structures, by taking advantage of the capability of ωFQ to correctly model the aforementioned graphene physical features.

To conclude, in this work we have presented a novel classical, fully atomistic approach, which we dub "ωFQ", to calculate the plasmonic properties of graphene-based nano- and microstructures. Its potential and performance have been tested by comparing results obtained by exploiting this approach, against *ab initio*, continuum, and experimental results. Several shapes and dimensions have been taken into consideration, showing that, pending a reliable parametrization of the classical frequency-dependent force field, an almost perfect agreement with either reference *ab initio* or experimental data is achieved. In particular, the limitations of the state-of-the-art approaches, i.e., purely classical continuum and QM-based models, are completely overcome, because ωFQ is able to treat realistic systems (∼370k atoms) by retaining the atomistic picture of the studied structures and by showing at the same time a perfect agreement with experimental data. Simultaneously, for smaller graphene sheets, ωFQ accuracy is perfectly in line with the best reference methods which have been presented in the literature. In addition, the development of ωFQ paves the way for an accurate description of the physicochemical properties of molecules adsorbed on graphene-based substrates, thus allowing a deep understanding of the nature of phenomena that have not been clearly explained, as for instance GERS.[16−19] Such an extension will require the coupling of ωFQ with a quantum mechanical (QM) description of the adsorbed molecule, in a QM/molecular mechanics (QM/MM) fashion.[46−51] Such a development will be the topic of future publications.

■ ASSOCIATED CONTENT

Supporting Information

The Supporting Information is available free of charge at https://pubs.acs.org/doi/10.1021/acs.jpclett.0c02051.

Detailed derivation of the ωFQ model for 2D substrates; model parametrization; structural details of the studied systems; validation of ωFQ model (PDF)

■ AUTHOR INFORMATION

Corresponding Author

Chiara Cappelli − *Scuola Normale Superiore, 56126 Pisa, Italy.*; orcid.org/0000-0002-4872-4505; Email: chiara.cappelli@sns.it

Authors

Tommaso Giovannini − *Department of Chemistry, Norwegian University of Science and Technology, 7491 Trondheim, Norway*; orcid.org/0000-0002-5637-2853

Luca Bonatti − *Scuola Normale Superiore, 56126 Pisa, Italy.*

Marco Polini − *Dipartimento di Fisica dell'Universitá di Pisa, I-56127 Pisa, Italy; Istituto Italiano di Tecnologia, Graphene Laboratories, 16163 Genova, Italy*

Complete contact information is available at: https://pubs.acs.org/10.1021/acs.jpclett.0c02051

Author Contributions

⊥T.G. and L.B. contributed equally to this work.

Notes

The authors declare no competing financial interest.

■ ACKNOWLEDGMENTS

This work has received funding from the European Research Council (ERC) under the European Union's Horizon 2020 research and innovation programme (Grant Agreement No. 818064). T.G. acknowledges funding from the Research Council of Norway through its grant TheoLight (Grant No. 275506). M.P. was supported by the European Union's

Horizon 2020 research and innovation programme under Grant Agreement No. 785219 - GrapheneCore2.

REFERENCES

(1) Geim, A. K.; Novoselov, K. S. *Nanoscience and Technology: A Collection of Reviews from Nature Journals*; World Scientific, 2010; pp 11−19.

(2) Grigorenko, A. N.; Polini, M.; Novoselov, K. S. Graphene plasmonics. *Nat. Photonics* **2012**, *6*, 749.

(3) García de Abajo, F. J. Graphene plasmonics: challenges and opportunities. *ACS Photonics* **2014**, *1*, 135−152.

(4) Woessner, A.; Lundeberg, M. B.; Gao, Y.; Principi, A.; Alonso-González, P.; Carrega, M.; Watanabe, K.; Taniguchi, T.; Vignale, G.; Polini, M.; Hone, J.; Hillenbrand, R.; Koppens, F.H. L. Highly confined low-loss plasmons in graphene−boron nitride heterostructures. *Nat. Mater.* **2015**, *14*, 421.

(5) Johnson, P. B.; Christy, R.-W. Optical constants of the noble metals. *Phys. Rev. B* **1972**, *6*, 4370.

(6) Ju, L.; Geng, B.; Horng, J.; Girit, C.; Martin, M.; Hao, Z.; Bechtel, H. A.; Liang, X.; Zettl, A.; Shen, Y. R.; Wang, F. Graphene plasmonics for tunable terahertz metamaterials. *Nat. Nanotechnol.* **2011**, *6*, 630.

(7) Fei, Z.; Rodin, A.; Andreev, G. O.; Bao, W.; McLeod, A.; Wagner, M.; Zhang, L.; Zhao, Z.; Thiemens, M.; Dominguez, G.; Fogler, M. M.; Neto, A. H. C.; Lau, C. N.; Keilmann, F.; Basov, D. N. Gate-tuning of graphene plasmons revealed by infrared nano-imaging. *Nature* **2012**, *487*, 82−85.

(8) Fei, Z.; Andreev, G. O.; Bao, W.; Zhang, L. M.; McLeod, A. S.; Wang, C.; Stewart, M. K.; Zhao, Z.; Dominguez, G.; Thiemens, M.; Fogler, M. M.; Tauber, M. J.; Castro-Neto, A. H.; Lau, C. N.; Keilmann, F.; Basov, D. N. Infrared nanoscopy of Dirac plasmons at the graphene−SiO2 interface. *Nano Lett.* **2011**, *11*, 4701−4705.

(9) Yan, H.; Li, X.; Chandra, B.; Tulevski, G.; Wu, Y.; Freitag, M.; Zhu, W.; Avouris, P.; Xia, F. Tunable infrared plasmonic devices using graphene/insulator stacks. *Nat. Nanotechnol.* **2012**, *7*, 330.

(10) Fang, Z.; Thongrattanasiri, S.; Schlather, A.; Liu, Z.; Ma, L.; Wang, Y.; Ajayan, P. M.; Nordlander, P.; Halas, N. J.; García de Abajo, F. J. Gated tunability and hybridization of localized plasmons in nanostructured graphene. *ACS Nano* **2013**, *7*, 2388−2395.

(11) Fang, Z.; Wang, Y.; Schlather, A. E.; Liu, Z.; Ajayan, P. M.; García de Abajo, F. J.; Nordlander, P.; Zhu, X.; Halas, N. J. Active tunable absorption enhancement with graphene nanodisk arrays. *Nano Lett.* **2014**, *14*, 299−304.

(12) Brar, V. W.; Jang, M. S.; Sherrott, M.; Lopez, J. J.; Atwater, H. A. Highly confined tunable mid-infrared plasmonics in graphene nanoresonators. *Nano Lett.* **2013**, *13*, 2541−2547.

(13) Chen, J.; Badioli, M.; Alonso-González, P.; Thongrattanasiri, S.; Huth, F.; Osmond, J.; Spasenović, M.; Centeno, A.; Pesquera, A.; Godignon, P.; Zurutuza Elorza, A.; Camara, N.; García de Abajo, F. J.; Hillenbrand, R.; Koppens, F. H. L. Optical nano-imaging of gate-tunable graphene plasmons. *Nature* **2012**, *487*, 77.

(14) Shin, S.; Kim, N.; Kim, J.; Kim, K.; Noh, D.; Kim, K. S.; Chung, J. Control of the π plasmon in a single layer graphene by charge doping. *Appl. Phys. Lett.* **2011**, *99*, No. 082110.

(15) Chen, C.-F.; Park, C.-H.; Boudouris, B. W.; Horng, J.; Geng, B.; Girit, C.; Zettl, A.; Crommie, M. F.; Segalman, R. A.; Louie, S. G.; Wang, F. Controlling inelastic light scattering quantum pathways in graphene. *Nature* **2011**, *471*, 617.

(16) Ling, X.; Xie, L.; Fang, Y.; Xu, H.; Zhang, H.; Kong, J.; Dresselhaus, M. S.; Zhang, J.; Liu, Z. Can graphene be used as a substrate for Raman enhancement? *Nano Lett.* **2010**, *10*, 553−561.

(17) Ling, X.; Zhang, J. First-Layer Effect in Graphene-Enhanced Raman Scattering. *Small* **2010**, *6*, 2020−2025.

(18) Ling, X.; Wu, J.; Xie, L.; Zhang, J. Graphene-thickness-dependent graphene-enhanced Raman scattering. *J. Phys. Chem. C* **2013**, *117*, 2369−2376.

(19) Ling, X.; Moura, L.; Pimenta, M. A.; Zhang, J. Charge-transfer mechanism in graphene-enhanced Raman scattering. *J. Phys. Chem. C* **2012**, *116*, 25112−25118.

(20) Koppens, F. H.; Chang, D. E.; García de Abajo, F. J. Graphene plasmonics: a platform for strong light−matter interactions. *Nano Lett.* **2011**, *11*, 3370−3377.

(21) Jablan, M.; Buljan, H.; Soljačić, M. Plasmonics in graphene at infrared frequencies. *Phys. Rev. B: Condens. Matter Mater. Phys.* **2009**, *80*, 245435.

(22) Vakil, A.; Engheta, N. Transformation optics using graphene. *Science* **2011**, *332*, 1291−1294.

(23) Thongrattanasiri, S.; Manjavacas, A.; García de Abajo, F. J. Quantum finite-size effects in graphene plasmons. *ACS Nano* **2012**, *6*, 1766−1775.

(24) Cox, J. D.; Silveiro, I.; García de Abajo, F. J. Quantum effects in the nonlinear response of graphene plasmons. *ACS Nano* **2016**, *10*, 1995−2003.

(25) Christensen, J.; Manjavacas, A.; Thongrattanasiri, S.; Koppens, F. H.; García de Abajo, F. J. Graphene plasmon waveguiding and hybridization in individual and paired nanoribbons. *ACS Nano* **2012**, *6*, 431−440.

(26) Grüneis, A.; Attaccalite, C.; Wirtz, L.; Shiozawa, H.; Saito, R.; Pichler, T.; Rubio, A. Tight-binding description of the quasiparticle dispersion of graphite and few-layer graphene. *Phys. Rev. B: Condens. Matter Mater. Phys.* **2008**, *78*, 205425.

(27) García de Abajo, F. J.; Howie, A. Retarded field calculation of electron energy loss in inhomogeneous dielectrics. *Phys. Rev. B: Condens. Matter Mater. Phys.* **2002**, *65*, 115418.

(28) Reich, S.; Maultzsch, J.; Thomsen, C.; Ordejon, P. Tight-binding description of graphene. *Phys. Rev. B: Condens. Matter Mater. Phys.* **2002**, *66*, No. 035412.

(29) Yan, J.; Thygesen, K. S.; Jacobsen, K. W. Nonlocal screening of plasmons in graphene by semiconducting and metallic substrates: first-principles calculations. *Phys. Rev. Lett.* **2011**, *106*, 146803.

(30) Brey, L.; Fertig, H. Electronic states of graphene nanoribbons studied with the Dirac equation. *Phys. Rev. B: Condens. Matter Mater. Phys.* **2006**, *73*, 235411.

(31) Brey, L.; Fertig, H. Elementary electronic excitations in graphene nanoribbons. *Phys. Rev. B: Condens. Matter Mater. Phys.* **2007**, *75*, 125434.

(32) Han, M. Y.; Özyilmaz, B.; Zhang, Y.; Kim, P. Energy band-gap engineering of graphene nanoribbons. *Phys. Rev. Lett.* **2007**, *98*, 206805.

(33) Bonatti, L.; Gil, G.; Giovannini, T.; Corni, S.; Cappelli, C. Plasmonic Resonances of Metal Nanoparticles: Atomistic vs. Continuum Approaches. *Front. Chem.* **2020**, *8*, 340.

(34) Giovannini, T.; Rosa, M.; Corni, S.; Cappelli, C. A classical picture of subnanometer junctions: an atomistic Drude approach to nanoplasmonics. *Nanoscale* **2019**, *11*, 6004−6015.

(35) Castro-Neto, A. H.; Guinea, F.; Peres, N. M.; Novoselov, K. S.; Geim, A. K. The electronic properties of graphene. *Rev. Mod. Phys.* **2009**, *81*, 109.

(36) Yan, H.; Low, T.; Zhu, W.; Wu, Y.; Freitag, M.; Li, X.; Guinea, F.; Avouris, P.; Xia, F. Damping pathways of mid-infrared plasmons in graphene nanostructures. *Nat. Photonics* **2013**, *7*, 394.

(37) Myroshnychenko, V.; Nishio, N.; García de Abajo, F. J.; Förstner, J.; Yamamoto, N. Unveiling and Imaging Degenerate States in Plasmonic Nanoparticles with Nanometer Resolution. *ACS Nano* **2018**, *12*, 8436−8446.

(38) Yu, R.; Cox, J. D.; Saavedra, J.; García de Abajo, F. J. Analytical modeling of graphene plasmons. *ACS Photonics* **2017**, *4*, 3106−3114.

(39) Manjavacas, A.; Thongrattanasiri, S.; García de Abajo, F. J. Plasmons driven by single electrons in graphene nanoislands. *Nanophotonics* **2013**, *2*, 139−151.

(40) Wang, H.; Wu, Y.; Lassiter, B.; Nehl, C. L.; Hafner, J. H.; Nordlander, P.; Halas, N. J. Symmetry breaking in individual plasmonic nanoparticles. *Proc. Natl. Acad. Sci. U. S. A.* **2006**, *103*, 10856−10860.

(41) Wang, H.; Brandl, D. W.; Nordlander, P.; Halas, N. J. Plasmonic nanostructures: artificial molecules. *Acc. Chem. Res.* **2007**, *40*, 53−62.

https://dx.doi.org/10.1021/acs.jpclett.0c02051
J. Phys. Chem. Lett. 2020, 11, 7595−7602

(42) Prodan, E.; Radloff, C.; Halas, N. J.; Nordlander, P. A hybridization model for the plasmon response of complex nanostructures. *Science* **2003**, *302*, 419−422.
(43) Bardhan, R.; Mukherjee, S.; Mirin, N. A.; Levit, S. D.; Nordlander, P.; Halas, N. J. Nanosphere-in-a-nanoshell: a simple nanomatryushka. *J. Phys. Chem. C* **2010**, *114*, 7378−7383.
(44) Park, T.-H.; Nordlander, P. On the nature of the bonding and antibonding metallic film and nanoshell plasmons. *Chem. Phys. Lett.* **2009**, *472*, 228−231.
(45) Radloff, C.; Halas, N. J. Plasmonic properties of concentric nanoshells. *Nano Lett.* **2004**, *4*, 1323−1327.
(46) Morton, S. M.; Silverstein, D. W.; Jensen, L. Theoretical studies of plasmonics using electronic structure methods. *Chem. Rev.* **2011**, *111*, 3962−3994.
(47) Payton, J. L.; Morton, S. M.; Moore, J. E.; Jensen, L. A hybrid atomistic electrodynamics−quantum mechanical approach for simulating surface-enhanced raman scattering. *Acc. Chem. Res.* **2014**, *47*, 88−99.
(48) Giovannini, T.; Puglisi, A.; Ambrosetti, M.; Cappelli, C. Polarizable QM/MM approach with fluctuating charges and fluctuating dipoles: the QM/FQFμ model. *J. Chem. Theory Comput.* **2019**, *15*, 2233−2245.
(49) Rinkevicius, Z.; Li, X.; Sandberg, J. A.; Mikkelsen, K. V.; Ågren, H. A hybrid density functional theory/molecular mechanics approach for linear response properties in heterogeneous environments. *J. Chem. Theory Comput.* **2014**, *10*, 989−1003.
(50) Cappelli, C. Integrated QM/Polarizable MM/Continuum Approaches to Model Chiroptical Properties of Strongly Interacting Solute-Solvent Systems. *Int. J. Quantum Chem.* **2016**, *116*, 1532−1542.
(51) Giovannini, T.; Grazioli, L.; Ambrosetti, M.; Cappelli, C. Calculation of IR Spectra with a Fully Polarizable QM/MM Approach Based on Fluctuating Charges and Fluctuating Dipoles. *J. Chem. Theory Comput.* **2019**, *15*, 5495−5507.

https://dx.doi.org/10.1021/acs.jpclett.0c02051
J. Phys. Chem. Lett. 2020, 11, 7595−7602